

Robust highly stable multi-resonator refractive index sensor

Myles Silfies, Dmitriy Kalantarov, Christopher P. Search *

Department of Physics and Engineering Physics, Stevens Institute of Technology, Castle Point on Hudson, Hoboken, NJ 07030, USA

ARTICLE INFO

Keywords:

Micro-optical devices
Integrated optics devices
Genetic algorithm
Index measurements

ABSTRACT

Here we show that a serial array of three evanescently coupled microring resonators can achieve detection limits for refractive index changes in the surrounding environment that are more than 40% better than a single resonator. The improved performance of the three rings occurs when only the central resonator is exposed to the refractive index change and is due to the narrower linewidth that results from the off-resonant coupling to the adjacent resonators. Unlike a single resonator sensor that is usually operated close to critical coupling to maximize the sensitivity, the three resonator configuration is able to achieve superior detection limits over a wide range of inter-resonator couplings. We use this to show that random variations of the couplings resulting from manufacturing variations has a minimal impact on the performance of the three ring system.

© 2017 Published by Elsevier B.V.

1. Introduction

Integrated microring resonators are one of several optical devices being developed as refractive index (RI) sensors [1–8] for the detection of biochemical analytes. The resonant wavelengths of the resonator are determined by the effective index of refraction, which itself is dependent on the index of refraction in the material surrounding the resonator waveguide due to the evanescent field of the resonator mode. The presence of an analyte, either in a bulk aqueous solution surrounding the resonator or attached to biorecognition elements on the resonator's surface, alters the index of refraction in the vicinity of the resonator. This leads to a shift of the resonant wavelength that can be detected with a tunable wavelength laser and spectrometer [9,10]. These micro-optical RI sensors have several advantages compared to more traditional detection techniques such as fluorescence including being cheaper, easier to operate, and label free [9].

Typically only a single ring resonator evanescently coupled to a waveguide in an all-pass configuration has been used. Moreover, the detection limit of the resonator decreases rapidly when the coupling to the waveguide deviates significantly from the critical coupling strength. Although the theoretical limit for the detection limit using a single resonator is 10^{-9} RIU (refractive index units), the best experimentally measured detection limit is only around 10^{-7} RIU [9]. By contrast, multi-resonator systems have found use as filters [11] and delay lines [12] due to the ability to control the shape and width of their transmission band as well as the phase delay using the inter-resonator evanescent couplings. The formation of transmission bands in arrays of coupled

resonators would appear to preclude them from RI sensing where it is desirable to have the narrowest possible transmission resonance. However, when one or more of the resonators have resonance frequencies incommensurate with the rest of the resonators, transmission resonances form that can be narrower than achievable by the lone resonator [13]. Unfortunately determining the parameters needed to achieve these narrower resonances is not straightforward.

For the work detailed in this paper, we theoretically model and analyze three microring resonators in series coupled evanescently to each other as represented by the fabricated device shown in Fig. 1 for RI sensing. The device in Fig. 1 serves only as a model for our theoretical analysis. Only the first resonator to the left is coupled to a waveguide through which the optical transmission is measured. The central resonator alone is exposed to the surrounding environment with the analyte and used to detect RI changes. The radius of the central resonator and its couplings to the adjacent resonators were treated as free variables that were optimized using a genetic algorithm to find a transmission resonance that maximizes the RI detection limit. We found that the three ring system is able to achieve a detection limit 41% better than the critically coupled single ring. However, what is also significant is the robustness of the three ring system to variations in any of the couplings since there exists a large range of values for the couplings that lead to performance better than a single ring RI sensor. We numerically simulated manufacturing defects by randomly varying the coupling coefficients of both the optimized three ring system and the single ring and showed that the three ring system's performance

* Corresponding author.

E-mail address: csearch@stevens.edu (C.P. Search).

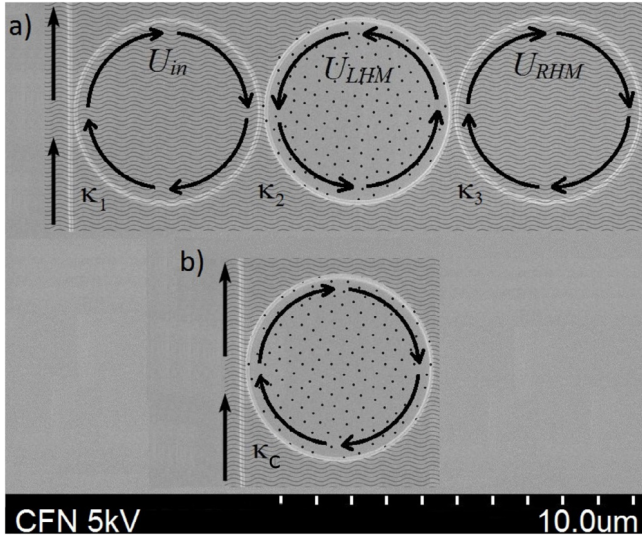


Fig. 1. (a) Three ring RI sensor in which only the central resonator is exposed to the analyte solution. The central resonator is evanescently coupled on both left and right sides to two additional resonators while only the leftmost resonator is coupled to a waveguide through which the transmission is measured. (b) Single micro-ring resonator RI index sensor coupled to waveguide in all pass geometry. Note the areas in waves are cladded and ones with dots are exposed to the analyte.

is less affected by the defects than the single ring and in most instances continues to show better detection limits than the optimized single ring.

2. Model

Fig. 1 provides a schematic of the RI sensor to be studied here. The device consists of a linear array of three evanescently coupled circular micro-ring resonators of radius R_j coupled to a waveguide in an all-pass configuration. The device is completely cladded except the central resonator, which is exposed to a solution containing the analyte. The presence of the analyte perturbs the RI surrounding the resonator and subsequently the effective index of the resonator mode thereby shifting the resonant wavelength λ_r . The effective index, n_{eff} , of the central resonator can be approximated as $n_{eff} \approx \eta n_s + (1 - \eta)n_c$, where η is the interaction coefficient measuring the fraction of the optical power in the evanescent field [9,10]. n_s is the index of the solution surrounding the resonator while the index of the resonator waveguide material is n_c . The presence of an analyte in the solutions will produce an index of refraction shift δn_s , which is proportional to both the concentration of the analyte and its molecular polarizability. The shift of the central resonator's resonant wavelength is then $\delta \lambda_r \approx \delta n_s (\eta \lambda_r / n_s)$ [9,10]. Note that in the numerical simulations presented below the effective index is calculated numerically using the model of an asymmetric waveguide [14].

To analyze the transmission through the waveguide coupled to the resonator array, we utilize the transfer matrix approach. As a result of phase matching, the light that is coupled from the waveguide into the clockwise (CW) whispering gallery mode of the first resonator will couple to the counter-clockwise (CCW) mode of the second resonator, which itself couples to the CW mode of the third resonator. The propagation of light in the CW and CCW directions and coupling to the nearest neighbor resonator are expressible in terms of transfer matrices [15,16]

$$U^{(1)} = \frac{-i}{\sqrt{K_1}} \begin{bmatrix} \sqrt{1-K_1}e^{i\phi_1} & -e^{i\phi_1} \\ e^{-i\phi_1} & -\sqrt{1-K_1}e^{-i\phi_1} \end{bmatrix} \quad (1)$$

$$U^{(2)} = \frac{i}{\sqrt{K_2}} \begin{bmatrix} \sqrt{1-K_2}e^{-i\phi_2} & -e^{-i\phi_2} \\ e^{i\phi_2} & -\sqrt{1-K_2}e^{i\phi_2} \end{bmatrix}, \quad (2)$$

$$U^{(3)} = \frac{-i}{\sqrt{K_3}} \begin{bmatrix} \sqrt{1-K_3}e^{i\phi_3} & -e^{i\phi_3} \\ e^{-i\phi_3} & -\sqrt{1-K_3}e^{-i\phi_3} \end{bmatrix}. \quad (3)$$

The transfer matrix for a signal propagating from the in port to the through port of the waveguide is expressible as

$$U = U^{(3)}U^{(2)}U^{(1)} = \begin{pmatrix} U_{11} & U_{12} \\ U_{21} & U_{22} \end{pmatrix}.$$

The transmission through the waveguide is given by

$$T = \left| \frac{U_{22} - U_{12}}{U_{11} - U_{21}} \right|^2, \quad (4)$$

which relates the output power in the through port to the input power at the in port, $P_{out} = T P_{in}$. In the matrices, $\phi_j = \beta_j \pi R_j$ is the propagation phase for the j th resonator with $\beta_j = \omega n_{eff} / c - i\alpha_j / 2$ for light of angular frequency ω and power attenuation per unit length α_j . K_2 and K_3 are the dimensionless power couplings between the first and second and second and third resonators, respectively while K_1 is the coupling between the waveguide and first resonator. Each of the K_j represent the fraction of the power coupled between the modes of the respective elements such that $0 \leq K_j \leq 1$ for $j = 1, 2, 3$. It is expressible in terms of an overlap integral between the mode functions in adjacent resonators and consequently depends on the cross-sectional dimensions of the resonators' waveguides and the spacing between resonators [17,18].

It is further assumed that the waveguide is excited from a tunable wavelength laser and that the transmitted spectrum is monitored with a spectrometer. The shift of the wavelength λ_c of the linecenter of a transmission resonance affected by the presence of the analyte is then measured. The sensitivity of the transmission resonance to a change in the index of refraction of the surrounding solution n_s is

$$S = \frac{d\lambda_c}{dn_s}, \quad (5)$$

which is in units of nm/RIU. In the case that the transmission resonance corresponds to the resonance wavelength of the central resonator, $\lambda_c = \lambda_r$ and $S \approx \eta \lambda_r / n_s$ [9]. The detection limit (DL), which is the minimum RI change that can be measured, is the ratio of the sensor resolution to the sensitivity. In our case the sensor would be a spectrometer that measures the shift of the line center of the resonance and the sensor resolution is therefore determined by both the spectral resolution of the spectrometer and any sources of noise that lead to an uncertainty in the position of the line center. Amplitude noise such as from the probing laser or thermal noise in the system will add to the resonance lineshape making it harder to identify the true extremum of the resonance representing the line center. The effect of noise on the resonance lineshape can be modeled using Monte Carlo simulations, which leads to the phenomenological equation for the detection limit described in Ref. [10],

$$DL = \frac{\Delta\lambda}{4.5S(SNR)^{0.25}} \quad (6)$$

where SNR is the signal to noise ratio which includes amplitude noise of the probing laser, thermo-optic noise of the resonator, and detector noise, and is chosen to be SNR = 80 dB for all simulations, which is equivalent to a shot-noise limited system with an input power $P_{in} = 1$ mW. Additionally, S is the sensitivity and $\Delta\lambda$ is the full-width at half-maximum (FWHM) of the resonances. It is worth emphasizing that the detection limit is not only determined by the sensitivity but also the linewidth of the resonance, which acts to filter the noise reducing the uncertainty in the measurement of the line center. Since the Q -factor of the resonance is $Q = \lambda_c / \Delta\lambda$ one can see that the detection limit scales as $DL \sim 1/SQ$, which is equivalent to other expressions given for the detection limit [19].

The optimal parameters presented here for the three ring sensor were found using a genetic algorithm running on a Tesla K40 graphics processing unit (GPU) that minimized the detection limit. In order to

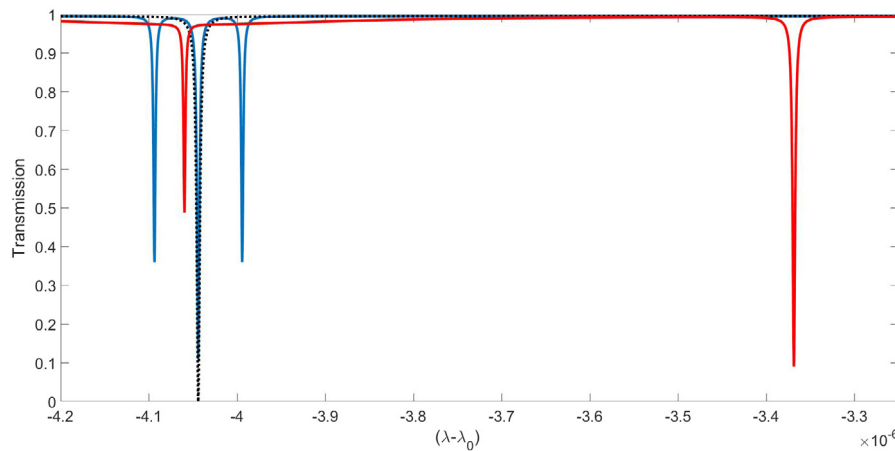


Fig. 2. Transmission spectrum for: three ring RI sensor with identical couplings $K_f^2 = 2\pi R\alpha$ and radii $R_f = 50 \mu\text{m}$ (solid blue line); single ring critically coupled RI sensor with $K_C^2 = 2\pi R\alpha$ and radius $R = 50 \mu\text{m}$ (dashed black line); optimized three ring RI sensor with $R_1 = R_3 = 50 \mu\text{m}$, $R_2 = 50.78 \mu\text{m}$ and coupling values given below in the text (solid red line). The material losses are in all cases $\alpha = 0.5 \text{ dB/cm}$.

simplify the optimization, the material losses in all resonators were fixed at $\alpha = 0.5 \text{ dB/cm}$. Additionally, the effective indices in the resonators were held at $n_{eff} = 1.46$ while a small variation at the central resonator of $\Delta n = 10^{-6}$ was used for the purpose of determining the sensitivity. The independent parameters that were optimized were the resonator radii and inter-resonator coupling coefficients. The genetic algorithm optimized the detection limit by mimicking the natural selection process found in biological evolution [20]. The algorithm works by establishing an initial population of randomly selected values for the independent parameters called “genes” which represent the system parameters and are repeatedly modified in successive generations “evolving” towards the lowest possible detection limit. During each generation, the detection limit produced by each member of the population is determined and only those with the best detection limits survive while the other population members are eliminated. The surviving population in each generation produce new offspring, which are modified by mixing of the parameters of two members of the population (breeding) and/or additional random variations of the parameters (mutation) [21–23]. The variables to be optimized in our genetic algorithm were the coupling coefficients K_f^2 and the radius of the central resonator which were stored in a vector, called a “chromosome”. Each chromosome representing a potential solution. The algorithm starts with an initially random population, then steps through a sequence of new generations created from the individuals in the current generation until the chromosome with lowest possible detection limit is found. The propagation of a new generation of chromosomes from the current generation was achieved by cycling through the following steps [24,25]:

(1) Members of the current population are evaluated and ranked based on their fitness (detection limit).

(2) The individuals having the best fitness are “cloned” and directly passed to the next generation.

(3) Parents are selected, based on their fitness and are “bred” to produce a child chromosome by taking a random convex combination of the parent vectors.

(4) Mutation, consisting of a random-point crossover and a Gaussian mutation was used to in order to introduce diversity into the population. For random-point crossover a random index, from 0 to $N - 1$ is chosen as the crossover point, for a vector of length N , and the two halves of the vector are swapped. While for Gaussian mutation consists of adding a random value from a Gaussian distribution to each element of an individual’s vector.

(5) Finally the current population is replaced with the next generation and the process is repeated.

In the end, only the radius of the central resonator was varied in the genetic algorithm while the other two radii were fixed at $50 \mu\text{m}$

since our initial investigations with the genetic algorithm indicated that symmetric distribution of the resonator radii had superior detection limits to asymmetric arrangements of the radii. After forming an initial population of 1000 by randomly selecting initial values for the central resonator radius and the three couplings, the algorithm passed the population array to the Nvidia GPU, which calculates the FWHM linewidth of the transmission resonances for only those whose contrast, defined as the difference between the maximum transmission far off resonance and minimum transmission at the linecenter, was at least 90%. To determine the sensitivity, the shift Δn in the index of refraction is introduced to the central resonator’s effective index and the transmission is recalculated to determine the wavelength shift of the resonances’ linecenter. From the FWHM and sensitivity, the detection limit of each resonance is calculated. All transmission resonances within a free spectral range of the resonators are evaluated in this way. The minimum detection limit achieved for each population member is then recorded along with the values of the independent parameters.

Once the minimum detection limits for the entire population were calculated, the population members were then sorted and ranked by the ratio of the contrast to detection limit of which the top 40% of candidates were cloned and continued to the next generation. Additionally, the top 30% were randomly “bred” with each other. Finally, 30% was mutated split evenly between random-point crossover and a Gaussian mutation. These percentages were chosen to insure that the algorithm did not become stuck at local minima but converged instead towards the global minimum of the detection limit in a reasonable time. Less breeding or mutation would have resulted in the algorithm getting stuck at detection limits that were local minima while significantly more mutation would have increased the number of generations needed to converge to the global minimum of the detection limit.

The above described process of passing to the GPU for calculation and then back to the CPU for analysis would then repeat with this new population which, when completed, would be compared to the current best candidates to find the best possible set of parameters for an index sensor [24,25]. This process would typically be repeated for several hundred to a thousand generations or until the top candidate remained unchanged for 20 generations.

3. Results

Fig. 2 shows the transmission spectrum in the case that all three resonators are the same radius R and all of the couplings are identical and equal to the critical coupling value of a single all pass resonator, $K_C^2 = 2\pi R\alpha$. The transmission of the single resonator using the same radius and coupling values is also shown for reference. For the three

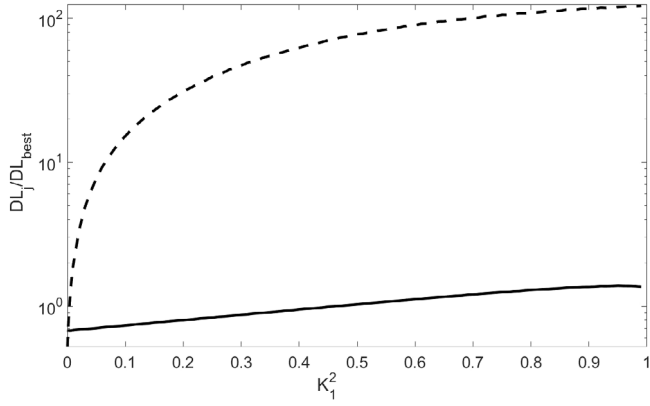


Fig. 3. Detection limit of the three ring system (solid line) and single ring system (dashed line) as a function of K_1^2 . The detection limit of both are measured relative to the detection limit of a single critically coupled all pass ring. For the three ring device $K_2^2 = 0.00371$, $K_3^2 = 0.03403$ also $R_1 = R_3 = 50 \mu\text{m}$ and a central resonator $R_2 = 50.775 \mu\text{m}$. The material losses are in all cases $\alpha = 0.5 \text{ dB/cm}$.

identical rings, one can see a triplet of closely spaced resonances with the spacing between them is proportional to K_C . Also shown is the transmission spectrum of the optimized three ring system having the lowest possible detection limit. The optimized three ring device was found to have couplings $K_1^2 = 0.4953$, $K_2^2 = 0.00371$, $K_3^2 = 0.03403$ and a central resonator with radius of $50.775 \mu\text{m}$ corresponding to a circumference that is $\lambda/2$ longer than the first and third resonators. The single resonance of the optimized system yields a RI detection limit 41% lower than that of the critically coupled single resonator of the same circumference. This improvement comes entirely from a reduction in the linewidth since its sensitivity of 0.125 nm/RIU is actually slightly worse than the critically coupled single ring, which is 0.134 nm/RIU .

However, what is more significant about the optimized three ring sensor is that it is able to achieve better detection limits over a very wide range of couplings, which would make it more robust to manufacturing variations and hence more practical for use. For example, Fig. 3 shows that the coupling of the first resonator to the waveguide K_1^2 has relatively little affect on the detection limit which changes by only $\pm 30\%$ over nearly the full range of K_1^2 from 10^{-4} to 0.99 . This is in sharp contrast to the single ring sensor whose detection limit rapidly worsens when the waveguide coupling deviates from K_C as seen by the dashed line in Fig. 3. The reason for such a stark difference between the two systems is that K_1^2 has almost no affect on the FWHM of the resonance for the three rings, which by contrast is primarily determined by the coupling and detuning of the central resonators to its neighbors. By contrast, the FWHM of the single resonator is determined exclusively by K_1^2 and the material losses and moreover the sensitivity varies significantly around the point of critical coupling [26,27]. Given that the waveguide coupling has very little effect on the detection limit of the three rings device, we set it to be $K_1^2 = 0.5$ corresponding to a 3 dB power coupler while varying K_2^2 and K_3^2 and measuring the resulting change in DL, which is shown in Fig. 4. It is clearly visible that the three rings have an extremely wide range of values for K_2^2 and K_3^2 for which DL is lower than that of the single ring system. Similar results were found for other values of K_1^2 .

To prove the robustness of the three ring system, we introduce disorder into our model by randomly varying the coupling coefficients, $K_j = K_{0,j} + \delta K_j$, where $K_{0,j}$ are the optimal values and δK_j are random fluctuations, which have zero mean and are modeled using a Gaussian distribution with a variance of $9K_C^2$. The same was also done for the critically coupled all pass single ring for which only the one coupling was randomly varied. We focus on variations of the coupling since the values of K_j are extremely sensitive to the separation between resonators due to the rapid attenuation of the evanescent field. By contrast the optical

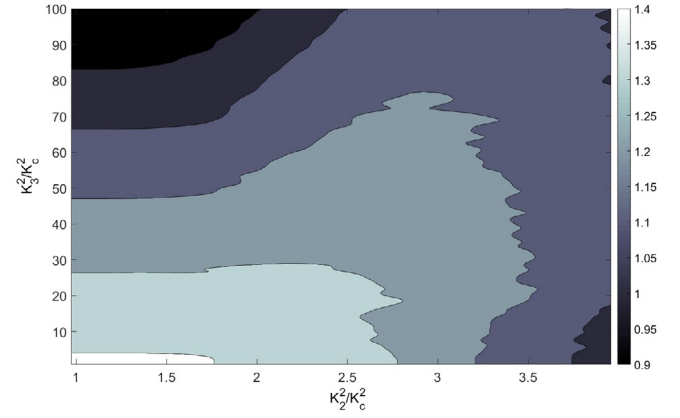


Fig. 4. Ratio of the detection limit of the critically coupled single ring to that of the three ring sensor as a function of K_2^2 and K_3^2 . The radii of the three ring system is the same as the optimum case and $K_1^2 = 0.5$.

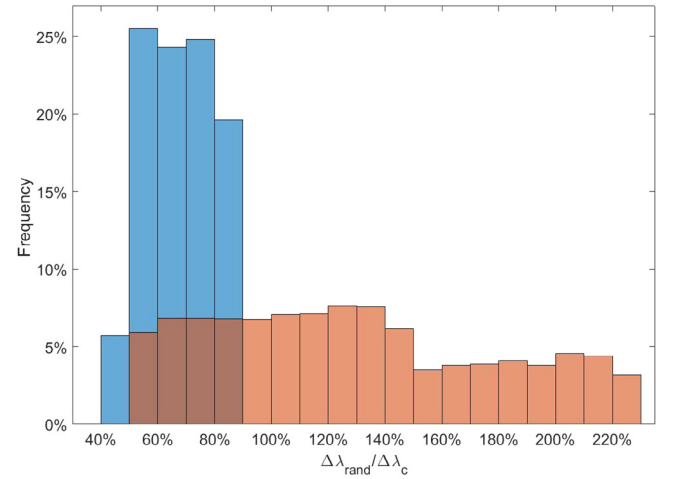


Fig. 5. Frequency of occurrence in the ensemble of different values of the FWHM linewidth $\Delta\lambda_3$ of the three ring sensor (blue bars) and single ring sensor $\Delta\lambda_1$ (orange bars) with random coupling coefficients measured relative to the FWHM linewidth $\Delta\lambda_C$ of the critically coupled single ring. Note that the radii of the three ring sensor are the same as the optimized case while for the single ring with random coupling the radius is the same as the critically coupled single ring.

path lengths of the resonators can be readily tuned post fabrication with techniques such as thermo-optic heaters. An ensemble of 10000 trials was generated in both cases from which the transmission spectra for each trial, $T^{(l)}$ was then calculated. From the transmission of each trial the linewidth of the resonance used for RI sensing, the sensitivity, and finally the detection limit were calculated.

Fig. 5 shows that for all elements of the ensemble, the linewidth of the three rings $\Delta\lambda_3$ is almost always narrower than the linewidth of the critically coupled single ring $\Delta\lambda_C$. In fact the average linewidth of the three rings is $\Delta\lambda_3 = 0.667\Delta\lambda_C$ while the standard deviation of the linewidth is only 11.5% of $\Delta\lambda_C$. By contrast, when random fluctuations are applied to the waveguide coupling of the single ring, the linewidth $\Delta\lambda_1$ is wider than $\Delta\lambda_C$ more than 60% of the time and more than a third of the times it is more than 50% wider with the average width being $\overline{\Delta\lambda_1} = 1.22\Delta\lambda_C$. The other factor besides linewidth that contributes to the detection limit is the sensitivity. For both systems, the sensitivities only varied by a few percent. In particular, for the three rings the average sensitivity was $0.93S_C$ with a standard deviation of $0.013S_C$ while for the single ring the average sensitivity was $1.01S_C$ and its standard deviation was $0.014S_C$ with $S_C = 0.134 \text{ nm/RIU}$ being the sensitivity of the critically coupled single ring.

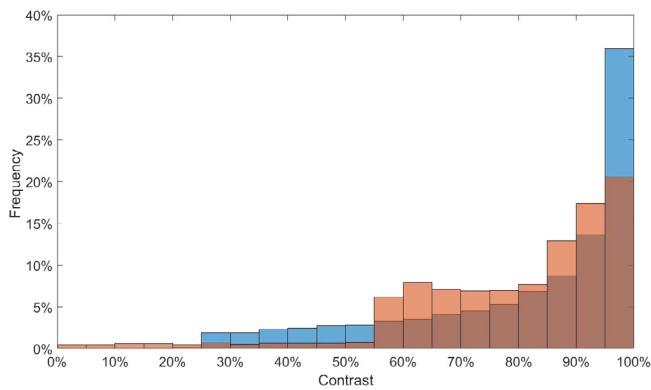


Fig. 6. Frequency of occurrence in the ensemble of different transmission contrasts of the three ring sensor (blue bars) and single ring sensor (orange bars) with random coupling coefficients. Note that the radii of the three ring sensor are the same as the optimized case while for the single ring with random coupling the radius is the same as the critically coupled single ring.

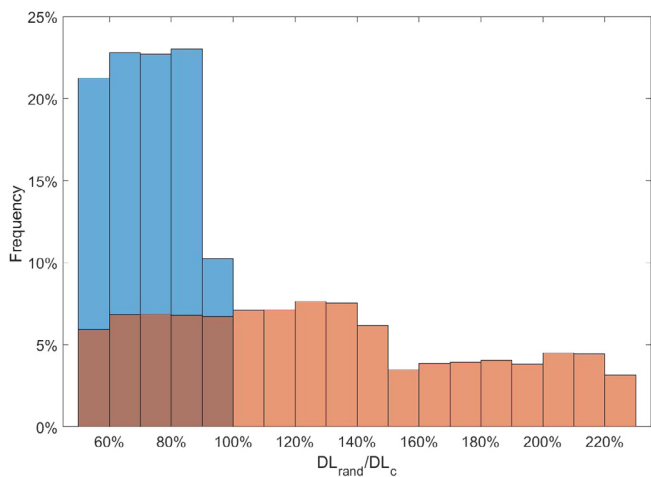


Fig. 7. Frequency of occurrence in the ensemble of different ratios of the detection limit of the three ring sensor DL_3 (blue bars) and single ring sensor DL_1 (orange bars) with random coupling coefficients to that of the critically coupled single ring DL_C . Note that the radii of the three ring sensor are the same as the optimized case while for the single ring with random coupling the radius is the same as the critically coupled single ring.

However, a narrower linewidth is of little value if the change in transmission from the line center to far off resonance is small, which is another reason why the single ring RI sensor is used closed to critical coupling since the transmission drops to zero at line center. To this end we looked at the contrast of the lines calculated as 1 minus the transmission at line center normalized to the optimal case for both devices. By this definition the critically coupled all pass single ring and the optimal three ring transmission of Fig. 2 both have 100% contrast. Fig. 6 shows the contrast of both when subject to perturbations in the couplings. The trend in both cases is towards lower contrast with the ensemble averaged contrast of the three rings being 81% while that of the single ring is 83%. However, for the three rings about 50% of the instances have contrasts of at least 90% while the single rings exhibit the same level of contrast in 45% of instances. Clearly the effect of the perturbations on the contrast is minimal for both devices.

Lastly, we look at the changes in the DL for both devices. Fig. 7 shows the ratio of DL for the perturbed devices to that of the critically coupled single ring, DL_C where one can see that DL of the perturbed three ring device is always at least as good or better than that of the critically coupled single ring. By contrast the perturbed single rings' detection limit is in more than 68% of instances worse than the critically coupled single ring, as one would expect. Although the perturbed single ring

in some instances has a DL lower than DL_C this is accompanied by a significant reduction in the contrast. More precisely, the average DL of the three ring system is $\overline{DL}_3 = 0.73 DL_C$ while the standard deviation is $0.13 DL_C$. By contrast, the average detection limit of the single resonator with perturbed coupling is $\overline{DL}_1 = 1.29 DL_C$ while the standard deviation is $0.49 DL_C$.

4. Discussion and conclusions

It is clear from the above analysis that the three resonator RI sensor is superior to that of a single resonator. We found that the three rings can achieve detection limits that are more than 40% better than that of the critically coupled single resonator provided the circumference of the central resonator being used for RI sensing is shifted by half of a wavelength relative to the adjacent resonators. Moreover, the detection limit of the three resonators is less affected by random fluctuations in the couplings than the single resonator. This is due to the narrower linewidth of the three ring system being more stable than the linewidth of the single ring since the sensitivity in both cases was only weakly affected by the fluctuations. This implies that the three resonator configuration will exhibit much greater flexibility in the choice of resonator couplings and show more resistance to manufacturing defects. This new configuration therefore has the potential to not only detect smaller analyte quantities but also be a more robust RI sensor.

Acknowledgment

This material is based on research carried out in part at the Center for Functional Nanomaterials, Brookhaven National Laboratory, which is supported by the U.S. Department of Energy, Office of Basic Energy Sciences, under Contract No. DE-AC02-98CH10886.

References

- [1] F. Morichett, C. Ferrari, A. Canciamilla, A. Melloni, The first decade of coupled resonator optical waveguides: Bringing slow light to applications, *Laser Photon. Rev.* 6 (1) (2012) 74–96.
- [2] J. Homola, S. Yee, G. Gauglitz, Surface plasmon resonance sensors: Review, *Sensors Actuators B: Chemical* 54 (1) (1999) 3–15.
- [3] E. Chow, A. Grot, L.W. Mirkarimi, M. Sigalas, G. Girolami, Ultracompact biochemical sensor built with two-dimensional photonic crystal microcavity, *Opt. Lett.* 29 (10) (2004) 1093–1095.
- [4] N.M. Hanumegowda, C.J. Stica, B.C. Patel, I.M. White, X. Fan, Refractometric sensors based on microsphere resonators, *Appl. Phys. Lett.* 87 (20) (2005) 201107.
- [5] L. Rindorf, J. Jensen, M. Dufva, L. Pedersen, P. Høiby, O. Bang, Photonic crystal fiber long-period gratings for biochemical sensing, *Opt. Express* 14 (18) (2006) 8224–8231.
- [6] W. Bogaerts, P.D. Heyn, T.V. Vaerenbergh, K.D. Vos, S.K. Selvaraja, T. Claes, P. Dumon, P. Bienstman, D.V. Thourhout, R. Baets, Silicon microring resonators, *Laser Photon. Rev.* 6 (1) (2012) 47–73.
- [7] M. Gabalis, D. Urbonas, R. Petruskevicius, A perforated microring resonator for optical sensing applications, *J. Opt.* 16 (10) (2014) 105003.
- [8] G.N. Tsigaridas, A study on refractive index sensors based on optical micro-ring resonators, *Photonics Sensors* 7 (3) (2017) 217–225.
- [9] C. Ciminelli, C. Campanella, F. Dell'Olio, C. Campanella, M. Armenise, Label-free optical resonant sensors for biochemical applications, *Prog. Quantum Electron.* 37 (2) (2013) 51–107.
- [10] I. White, X. Fan, On the performance quantification of resonant refractive index sensors, *Opt. Express* 16 (2) (2008) 1020–1028.
- [11] B. Little, S. Chu, P. Absil, J. Hryniewicz, F. Johnson, F. Seiferth, D. Gill, V. Van, O. King, M. Trakalo, Very high-order microring resonator filters for WDM applications, *IEEE Photonics Technol. Lett.* 16 (10) (2004) 2263–2265.
- [12] J. Poon, L. Zhu, G. DeRose, A. Yariv, Transmission and group delay of microring coupled-resonator optical waveguides, *Opt. Lett.* 31 (4) (2006) 456–458.
- [13] S. Longhi, Tunable dynamic Fano resonances in coupled-resonator optical waveguides, *Phys. Rev. A* 91 (6) (2015) 063809.
- [14] A. Yariv, P. Yeh, *Photonics: Optical Electronics in Modern Communications*, vol. 6, Oxford University Press, New York, 2007.
- [15] J.K.S. Poon, J. Scheuer, S. Mookherjee, G.T. Palocz, Y. Huang, A. Yariv, Matrix analysis of microring coupled-resonator optical waveguides, *Opt. Express* 12 (1) (2004) 90–103.
- [16] J. Capmany, P. Muñoz, J.D. Domenech, M.A. Muriel, Apodized coupled resonator waveguides, *Opt. Express* 15 (16) (2007) 10196–10206.

- [17] D. Marcuse, Directional couplers made of nonidentical asymmetric slabs. Part I: Synchronous couplers, *J. Lightwave Technol.* 5 (1) (1987) 113–118.
- [18] G. Gupta, Y.H. Kuo, H. Tazawa, W.H. Steier, A. Stapleton, J.D.O. Brien, Analysis and demonstration of coupling control in polymer microring resonators using photobleaching, *Appl. Opt.* 48 (28) (2009) 5324–5336.
- [19] T. Yoshie, L. Tang, S.-Y. Su, Optical microcavity: Sensing down to single molecules and atoms, *Sensors* 11 (2011) 1972–1991.
- [20] O. Kramer, *Genetic Algorithm Essentials*, vol. 679, Springer, 2017.
- [21] P. Chamorro-Posada, R. Gómez-Alcalá, F.J. Fraile-Peláez, Study of optimal all-pass microring resonator delay lines with a genetic algorithm, *J. Lightwave Technol.* 32 (8) (2014) 1477–1481.
- [22] B. Bhowmik, S. Gupta, R. Gangopadhyay, Enhancement of the equalization range in a nonlinear micro-ring resonator based all-optical packet power equalizer using a genetic algorithm, *J. Opt.* 14 (7) (2012) 075502.
- [23] A. Bahrapour, F. Bazouband, V. Nickfarjam, Effect of direct coupling of microrings on the gain bandwidth of cascade microring Raman amplifier, *Opt. Commun.* 283 (14) (2010) 2939–2946.
- [24] J. Goh, I. Fushman, D. Englund, J. Vučković, Genetic optimization of photonic bandgap structures, *Opt. Express* 15 (13) (2007) 8218–8230.
- [25] L. Rosa, K. Saitoh, K. Kakiyama, M. Koshib, Genetic-algorithm assisted design of C-band CROW-miniaturized PCW interleaver, *J. Lightwave Technol.* 27 (14) (2009) 2678–2687.
- [26] W. Zhang, S. Serna, X.L. Roux, L. Vivien, E. Cassan, Highly sensitive refractive index sensing by fast detuning the critical coupling condition of slot waveguide ring resonators, *Opt. Lett.* 41 (3) (2016) 532–535.
- [27] S. Chandran, R.K. Gupta, B.K. Das, Dispersion enhanced critically coupled ring resonator for wide range refractive index sensing, *IEEE J. Sel. Top. Quantum Electron.* 23 (2) (2017) 1–9.